

FIG. 1. Time evolution of the (a) local and (b) integrated OTOC in the special Clifford circuit discussed in the text, demonstrating the generic behavior expected in a one-dimensional system with local interactions. Early time growth is characterized by a Lyapunov exponent λ_L , while at late times the growth of the iOTOC is linear, with a rate determined by the butterfly velocity v_B and the saturation value of local OTOC, C_{sat} . The crossover time between the two regimes (the scrambling time) is indicated by t_* .

tial growth, and characterize the crossover time to the saturated regime. Numerical results for this model are complemented by analytic rate equation which provide further insights on the temporal profile of the integrated OTOC. We then consider more generic Clifford and non-Clifford circuits, and show that our main results remain unchanged.

Scrambling time in systems with local interactions.- We consider a finite-dimensional system defined on a lattice, where each lattice site contains a degree of freedom with a finite-dimensional Hilbert space. The OTOC of two local operators, W_i, V_j , acting on sites i, j respectively, is given by

$$C_{i,j}(t) = - \left\langle [W_i(t), V_j]^2 \right\rangle. \quad (1)$$

Since in this work we focus on a random unitary circuit evolution, for which there is no well-defined notion of temperature, we take the expectation value above to be over an ensemble of random states, corresponding to the infinite temperature limit. While our arguments hold for systems of an arbitrary finite spatial dimension, for simplicity, we will focus on the one-dimensional case below and address higher dimensions later on. In a generic scenario, upon time evolution, the support of the operator $W_i(t)$ grows ballistically, forming a light cone with the front propagating at the butterfly velocity v_B . The OTOC above becomes finite once the site j enters this light cone. Following an early exponential growth regime, the value of $C_{i,j}(t)$ must saturate at late times, as its value is bounded due to the finite dimension of the local Hilbert space. This behavior is shown in Fig. 1(a), for a random circuit model to be described below.

While the structure and dynamics of the local OTOC (1) are interesting on their own right, here we would like to focus on the global properties of the scrambling dynamics. To this end, we introduce the integrated OTOC (iOTOC),

$$f(t) = \sum_j C_{i,j}(t) = - \sum_j \left\langle [W_i(t), V_j]^2 \right\rangle, \quad (2)$$

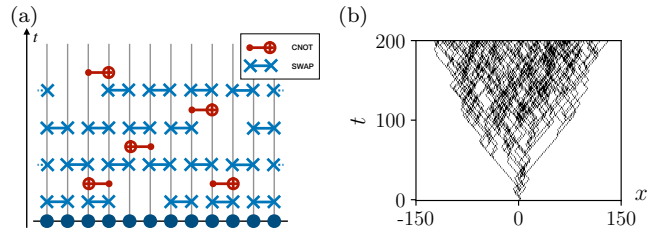


FIG. 2. (a) Schematic representation of the Clifford unitary circuit. At odd (even) time steps a set of SWAP gates is applied on odd (even) bonds with probability p on each bond, followed by a set of CNOT gates which are applied on a fraction r of the bonds. (b) Density of σ^z operators in the operator string $\sigma_0^z(t)$, for a single realization of the circuit with $p = 0.9, r = 0.05$.

where a summation is performed over all the lattice sites of the system [43]. The iOTOC measures the expectation value of the “size” of the operator [44, 45], washing out any transient behaviors and details of spatial structure, and thus simplifying the identification and characterization of the scrambling time in systems with local structure. Similarly to the local OTOC, at early times, we expect the iOTOC to exhibit an exponential growth characterized by a Lyapunov exponent $f(t) \sim e^{\lambda_L t}$. At late times, when the OTOC in the bulk of the system reaches its saturation value C_{sat} , the iOTOC crosses over to a linear growth regime (due to the linear growth of the size of the light cone), $f(t) \sim C_{\text{sat}} v_B t$. Assuming a single crossover time t_* (the scrambling time) between these two regimes, it can be obtained from

$$e^{\lambda_L t_*} \sim c_{\text{sat}} v_B t_* \Rightarrow t_* \sim \frac{1}{\lambda_L} \log \frac{C_{\text{sat}} v_B}{\lambda_L}, \quad (3)$$

where we introduced the OTOC density at saturation $c_{\text{sat}} = C_{\text{sat}}/a$, with a being the lattice spacing. We thus find, that a parametrically long scrambling time is expected for a diverging ratio v_B/λ_L , allowing for a prolonged time window where an exponential growth regime could be observed in systems with local structure. The iOTOC, corresponding to the local OTOC shown in Fig. 1(a), is plotted in Fig. 1(b), where this behavior can be observed.

Random Clifford circuit model.- To demonstrate the arguments above, we study the scrambling dynamics in a random unitary circuit. We start with the simplest circuit model in which the general behavior discussed above can be observed, and which is amenable to both analytical and large scale numerical analysis. A study of a more generic version of the circuit, which concurs with the results obtained here, is presented later on. The structure of the circuit we consider here is shown schematically in Fig. 2(a). At every odd (even) time step a set of SWAP gates is applied on the odd (even) bonds, with probability $0 \leq p \leq 1$ on each bond. A SWAP gate interchanges the state of the two qubits it acts on, and can be written explicitly as $\sigma_1^+ \sigma_2^- + \sigma_1^- \sigma_2^+ + (1 + \sigma_1^z \sigma_2^z)/2$, where σ^\pm and σ^z are Pauli operators. Then, a set of CNOT gates is

applied on a fraction $0 \leq r \leq 1/2$ of all the bonds. The bonds are chosen such that only configurations where no two bonds share a site are allowed and each such configuration is equally probable. The role of each qubit (control or target) is chosen randomly and independently for each pair of sites.

First, note that the circuit consists of Clifford gates only and therefore can be simulated classically [46], allowing us to explore large system sizes and long times. Upon Clifford evolution, an operator $\sigma_i^\alpha(t=0) = \sigma_i^\alpha$, with $\alpha = x, y, z$, remains a single operator string of Pauli operators. In particular, for the circuit structure described above, when the operator $\sigma_i^z(t)$ is considered, the corresponding operator string at times $t > 0$ consists only of σ^z and identity operators, as we will see below. Fig. 2(b) shows the density of σ^z operators in this case as a function of time, for a single realization of the circuit.

To better understand the evolution of operators in this circuit consider first the limit of $r = 0$ (i.e. in the absence of CNOT gates), and $p = 1$ (i.e. when the SWAP gates are applied on all odd / even bonds at each time step). In this case, a single-site operator located on an odd (even) site of the 1D chain, will propagate ballistically to the right (left) with velocity $v_{B,0} = 1$. Decreasing p can be thought of as introducing disorder, as a missing SWAP gate results in a back-scattering of an operator, flipping its velocity. This gives rise to a diffusive propagation with diffusion constant $D \sim v_{B,0}^2 \tau_p$, where $\tau_p \sim (1-p)^{-1}$ is the characteristic time between consecutive back-scatterings.

Next, consider a finite $r > 0$, and for concreteness focus on the evolution of a σ^z operator. The action of a CNOT gate on operators (when the first qubit is the control qubit and the second one is the target) is given by

$$\sigma^z \otimes \mathbb{1} \rightarrow \sigma^z \otimes \mathbb{1}, \mathbb{1} \otimes \sigma^z \rightarrow \sigma^z \otimes \sigma^z, \sigma^z \otimes \sigma^z \rightarrow \mathbb{1} \otimes \sigma^z. \quad (4)$$

This process can be thought of as a scattering event for the operators due to interactions, which increases the support of a local operator. Denoting the scattering time due to the CNOT gates as $\tau_r \sim r^{-1}$, we note that in the diffusive case ($p < 1$), a finite r gives rise to a finite butterfly velocity $v_B \sim \sqrt{D/\tau_r} \sim \sqrt{r/(1-p)}$ [37].

We are interested in the evolution of the OTOC in this circuit. Writing the operator string corresponding to $\sigma_i^\alpha(t)$ explicitly as $\otimes_k \sigma_k^{\alpha_k(t)}$ (where k runs over all the sites of the 1D system, and we use σ^0 to denote the identity), the commutator $[\sigma_i^\alpha(t), \sigma_j^\beta]$ is given by $(\otimes_{k \neq j} \sigma_k^{\alpha_k(t)}) \otimes [\sigma_j^{\alpha_j(t)}, \sigma_j^\beta]$. Since $(\sigma_k^{\alpha_k(t)})^2 = \mathbb{1}$ for any $\alpha_k(t)$, the commutator squared is simply $[\sigma_j^{\alpha_j(t)}, \sigma_j^\beta]^2 = 4(\delta_{\beta, \alpha_j(t)} - 1)\mathbb{1}$ for $\alpha_j(t) \neq 0$ (i.e. $\sigma_j^{\alpha_j(t)} \neq \mathbb{1}$). In particular, the expectation value is state independent. Performing the summation over j in Eq. (2) with $W_i = \sigma_i^\alpha/\sqrt{2}$ and $V_j = \sigma_j^\beta/\sqrt{2}$, we find $f(t) = \sum_j (1 - \delta_{\beta, \alpha_j(t)})(1 - \delta_{\alpha_j(t), 0})$, i.e. the number of (non-identity) Pauli operators in $\sigma_i^\alpha(t)$ which are different from σ^β . For concreteness, below, we will consider the OTOC between $\sigma_i^z(t)$ and σ_j^x , so that

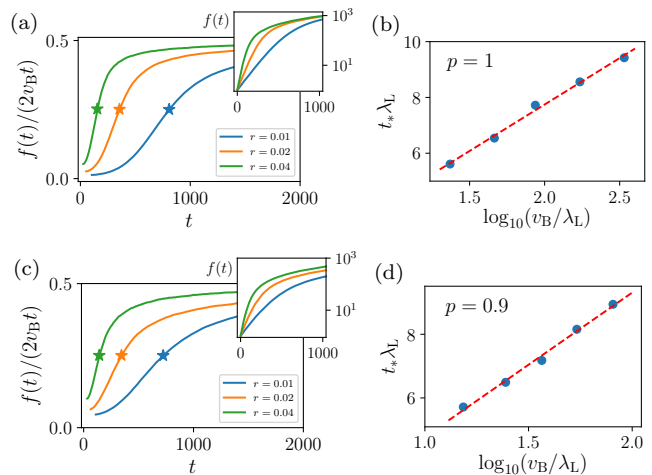


FIG. 3. Numerical results for the OTOC in the Clifford circuit, for the ballistic case ($p = 1$) in (a,b), and for the diffusive case ($p = 0.9$) in (c,d). (a,c) The OTOC density, $f(t)/(2v_B t)$, for different values of r as function of time. The crossover time, t_* , when the OTOC density reaches half of the saturation value, is indicated by a star. Insets: $f(t)$ on a log scale. (b,d) Scaling of t_* with λ_L (extracted as the slope of the integrated OTOC at early times) and v_B (extracted from the spatial profile of the operator density at late times).

$f(t)$ amounts to the number of σ^z operators in the string $\sigma_i^z(t)$ at time t . Note that the commutator $[\sigma_i^z(t), \sigma_j^z]$ vanishes identically for any realization of the circuit in this model. In fact, any state which is a product state in the z basis remains un-entangled upon evolution with the circuit above. However, this property of the circuit is not important for the discussion below, and we will show later on that our results hold for the more generic case as well.

Numerical results for integrated OTOCs and crossover time. - We now study the behavior of the iOTOC in this model as function of the circuit parameters. To this end, we perform numerical simulations of the operator dynamics, calculating the local and integrated OTOC. As was already mentioned, the density of the CNOT gates, r , is the parameter that sets the growth rate of the support of a local operator in the circuit and leads to scrambling. Therefore, we expect the Lyapunov exponent λ_L to be directly determined by r . In the limit $r \ll 1$ (and hence large v_B/λ_L), we expect an extended time regime in which the growth of the iOTOC is exponential with a well-defined Lyapunov exponent. We find that this is indeed the case both for the ballistic and the diffusive parameter regime, as can be seen in the insets of Figs. 3(a,c). To further analyze the crossover time, and its scaling with λ_L and v_B , we look at the average OTOC density, namely the iOTOC, $f(t)$, divided by the size of the light cone, $2v_B t$ (see Figs. 3(a,c)). At late times we expect this quantity to approach the saturation value of the OTOC in the bulk, which we find to be $1/2$ and independent of r in the regime $r \ll 1$. (This value is in agreement with the expectation

from the analytic rate equation analysis presented later on.) We define the crossover time t_* as the time at which the averaged OTOC density reaches half of its saturation value. In Figs. 3(b,d) we show that the crossover time extracted as above, indeed obeys the scaling expected from Eq. (3) both for the ballistic circuit with $p = 1$ and the diffusive one with $p = 0.9$. The results were obtained by averaging over $4 \cdot 10^3$ (10^4) realizations for the ballistic (diffusive) case.

Master equation for integrated OTOC.- To gain further insights on the scrambling process in the model described above, we now derive analytic rate equations for the iOTOC. We consider the limit of small but finite r , and $1 - p \ll 1$, such that the scattering events due to the CNOT gates are dilute and can be assumed to be uncorrelated [47]. This assumption is analogous to the molecular chaos hypothesis.

At time step t , the number of CNOT gates applied within the light cone of an operator $\sigma_i^z(t)$ is $N_{\text{CNOT}} = 2rv_B t$. Consider what happens to the total number of σ^z operators in the operator string upon application of a CNOT gate. From (4), we see that this number increases by one if the target (but not the control) site hosts a σ^z operator, while if both sites host a σ^z operator, the number decreases by one. Denote the fraction of non-identity operators in the operator string of $\sigma_i^z(t)$, within its light cone, by $q \equiv f(t)/(2v_B t)$. Assuming the probabilities of different sites to host a σ^z operator are independent, the probabilities for the processes which increase or decrease the number of non-identity operators in the string are given by $q(1 - q)$ and q^2 , respectively. Thus, the change in the number of σ^z operators in the operator string in a single time step is given by $N_{\text{CNOT}}(q(1 - q) - q^2)$. Recalling that the iOTOC is given simply by the number of non-identity operators in the operator string, as discussed above, we find that the rate equation for the iOTOC is (treating the time as continuous)

$$\frac{df}{dt} = rf(t) \left(1 - \frac{f(t)}{v_B t}\right). \quad (5)$$

This equation admits a solution of the form

$$f(t) = \frac{g_0 e^{rt}}{1 + g_0 \frac{r}{v_B} [\text{Ei}(rt) - \text{Ei}(1)]}, \quad (6)$$

where $\text{Ei}(rt)$ is the exponential integral, and g_0 is a constant set by the initial conditions. At early times, we see that indeed $f(t) \sim e^{\lambda_L t}$, with a Lyapunov exponent set by the CNOT gates density, $\lambda_L = r$. At late times, using the asymptotic expansion for the exponential integral, we find $f(t) \simeq v_B t / (1 + (rt)^{-1})$, i.e. the slope asymptotically approaches the butterfly velocity. The average OTOC density, $f(t)/(2v_B t)$ thus tends to 1/2 as observed numerically (see Figs. 3(a,c)). The crossover time, t_* , at which the OTOC density reaches a finite fraction of the saturation value, is given (to leading order) by $e^{rt_*} \sim v_B t_*$ in agreement with Eq. (3) and as observed numerically. Although the focus of our discussion here was

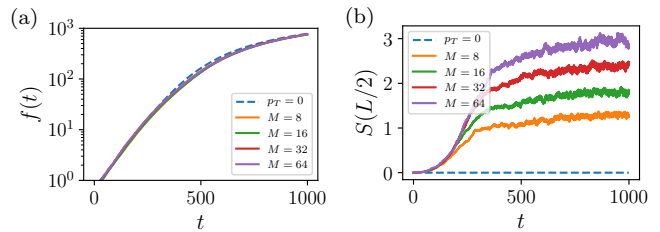


FIG. 4. (a) Integrated OTOC obtained for the generalized circuit models, shown on a log-scale, and (b) operator entanglement entropy across the middle bond in the system, as function of time, for different bond dimensions M . Averaging over 300 realizations of the circuit is performed in each case. The dashed line corresponds to the generalized Clifford evolution, in the absence of T gates (in this case operator entanglement remains zero at all times).

on the iOTOC, in which the spatial structure is washed out, in the Supplementary Material (SM) [47] we discuss hydrodynamic equations capturing the spatial structure and discuss their validity. We observe a crossover from a propagation in which the front maintains its shape to a regime where the front broadens diffusively.

Generalizations of the random circuit model.- As noted previously, the circuit model considered above is a special type of a Clifford circuit, in which both operator entanglement and state entanglement do not grow upon time evolution. We now demonstrate that our results do not rely on either of these properties. For simplicity, we restrict the analysis below to the ballistic case, i.e. $p = 1$.

First, consider a generalization of the circuit, in which the standard CNOT gate is replaced by a CNOT operation where the basis for both the control and the target qubits is chosen to be the x,y or z basis randomly and independently for each of the two qubits. Namely

$$U_{\text{CNOT}}^{\alpha,\beta} = \frac{\mathbb{1}_1 + \sigma_1^\alpha}{2} \otimes \mathbb{1}_2 + \frac{\mathbb{1}_1 - \sigma_1^\alpha}{2} \otimes e^{i\frac{\pi}{4}\sigma_2^\beta}, \quad (7)$$

where $\alpha, \beta \in x, y, z$. While this remains a Clifford circuit, the entanglement of a state generically grows with time in this case. We consider the averaged OTOC $\propto \sum_{\mu,\nu=x,y,z} \langle [\sigma_i^\mu(t), \sigma_j^\nu]^2 \rangle$. The averaged iOTOC obtained for this model, for CNOT gate density $r = 0.01$, is plotted in Fig. 4(a) (dashed blue line). It can be seen that a prolonged regime of exponential growth is present, similarly to the simplified model. Additional results for this model, and in particular a verification of the scaling in Eq. (3), are given in the SM [47].

We next consider a further generalization to a non-Clifford circuit. To this end, at each time step of the evolution, following the application of CNOT gates, a T gate (i.e. a $\pi/4$ phase gate, around a randomly chosen axis) is applied with probability p_T at each site. To calculate the OTOCs in presence of T gates we perform the time evolution of operators using a matrix product state (MPS) [48] representation of the operator string, employing the ITensor library [49]. Due to the exponential

growth of operator entanglement exact simulations are limited to short times. To go to longer times we perform truncation of the MPS bond dimension. In Fig. 4(a) we plot the iOTOC for $r = 0.01$ and T gate density $p_T = 0.01$, for different maximal bond dimensions. The respective operator entanglement that builds up in the system is shown in Fig. 4(b). We see that although the operator entanglement in the system is now non-zero, the iOTOCs are essentially unmodified. Note that evolution up to times $t \sim 300$ is carried out without any truncation, and is thus exact.

Discussion.- In this work we proposed a condition for the existence of a Lyapunov exponent in many-body systems with local interactions and a finite dimensional on-site Hilbert space. Having a parametrically long scrambling time (where the OTOC is exponentially growing, and hence λ_L is well-defined) requires the ratio v_B/λ_L to be large. This condition is naturally fulfilled in weakly coupled systems. Whether the condition is satisfied in other situations, e.g., in generic strongly-coupled systems in the low-temperature limit, remains to be seen.

Our condition is demonstrated in an explicit one-dimensional random unitary circuit model, where we have verified the relation between the scrambling time and v_B/λ_L . However, we expect the results to carry over to higher dimensions. Since the number of sites in the light cone grows as $(v_B t)^d$ in the d -dimensional case, the late-time iOTOC scales as $f(t) \sim t^d$. Therefore, the parametrically large scrambling time is enhanced by a factor of d relative to the one-dimensional case.

Finally, we note that other probes for scrambling have been proposed, in particular the growth of state and op-

erator entanglement [9–14, 20, 22]. In our Clifford circuit, we find an exponential growth of the OTOC despite the fact that the operator entanglement (as well as the state entanglement in the special circuit described above) do not grow, indicating that the existence of a Lyapunov exponent captures a different aspect of scrambling.

ACKNOWLEDGMENTS

Acknowledgements- We thank Ehud Altman, Bela Bauer, Eduardo Fradkin, Dima Pikulin, Steve Shenker, and Brian Swingle for stimulating discussions. This research is funded in part by the Gordon and Betty Moore Foundation through Grant GBMF8690 to UCSB to support the work of A.K. in KITP. Use was made of the computational facilities administered by the Center for Scientific Computing at the CNSI and MRL (an NSF MRSEC; DMR-1720256) and purchased through NSF CNS-1725797. L.N. is supported by the Kadanoff Fellowship at the University of Chicago and NSF grant DMR-1725401 at the University of Illinois. EB was supported by the European Research Council (ERC) under grant HQMAT (grant no. 817799), by the Israel Science Foundation Quantum Science and Technology grant no. 2074/19, and by CRC 183 of the Deutsche Forschungsgemeinschaft. We thank the hospitality of the Kavli Institute for Theoretical Physics, supported by the NSF under Grant No. NSF PHY-1748958, and the Aspen Center for Physics, supported by NSF grant PHY-1607611, where parts of this work were performed.

-
- [1] J. M. Deutsch. Quantum statistical mechanics in a closed system. *Phys. Rev. A*, 43:2046–2049, Feb 1991.
 - [2] Mark Srednicki. Chaos and quantum thermalization. *Phys. Rev. E*, 50(2):888–901, Aug 1994.
 - [3] D.M. Basko, I.L. Aleiner, and B.L. Altshuler. Metal-insulator transition in a weakly interacting many-electron system with localized single-particle states. *Annals of Physics*, 321(5):1126 – 1205, 2006.
 - [4] Arijeet Pal and David A. Huse. Many-body localization phase transition. *Phys. Rev. B*, 82:174411, Nov 2010.
 - [5] D. A. Roberts and D. Stanford. Diagnosing Chaos Using Four-Point Functions in Two-Dimensional Conformal Field Theory. *Physical Review Letters*, 115(13):131603, September 2015.
 - [6] S. H. Shenker and D. Stanford. Black holes and the butterfly effect. *Journal of High Energy Physics*, 3:67, March 2014.
 - [7] J. Maldacena, S. H. Shenker, and D. Stanford. A bound on chaos. *Journal of High Energy Physics*, 8:106, August 2016.
 - [8] J. S. Cotler, G. Gur-Ari, M. Hanada, J. Polchinski, P. Saad, S. H. Shenker, D. Stanford, A. Streicher, and M. Tezuka. Black holes and random matrices. *Journal of High Energy Physics*, 5:118, May 2017.
 - [9] P. Hosur, X.-L. Qi, D. A. Roberts, and B. Yoshida. Chaos in quantum channels. *Journal of High Energy Physics*, 2:4, February 2016.
 - [10] Xiao Chen and Tianci Zhou. Operator scrambling and quantum chaos, 2018.
 - [11] Mike Blake and Noah Linden. Quantum circuits with classically simulable operator scrambling, 2020.
 - [12] Laimei Nie, Masahiro Nozaki, Shinsei Ryu, and Mao Tian Tan. Signature of quantum chaos in operator entanglement in 2d CFTs. *arXiv e-prints*, page arXiv:1812.00013, Nov 2018.
 - [13] Cheryne Jonay, David A. Huse, and Adam Nahum. Coarse-grained dynamics of operator and state entanglement, 2018.
 - [14] Adam Nahum, Jonathan Ruhman, Sagar Vijay, and Jeongwan Haah. Quantum entanglement growth under random unitary dynamics. *Phys. Rev. X*, 7:031016, Jul 2017.
 - [15] Daniel E. Parker, Xiangyu Cao, Alexander Avdoshkin, Thomas Scaffidi, and Ehud Altman. A universal operator growth hypothesis. *Phys. Rev. X*, 9:041017, Oct 2019.
 - [16] Pavel Kos, Marko Ljubotina, and Tomaž Prosen. Many-body quantum chaos: Analytic connection to random matrix theory. *Phys. Rev. X*, 8:021062, Jun 2018.
 - [17] Amos Chan, Andrea De Luca, and J. T. Chalker. Spectral

- statistics in spatially extended chaotic quantum many-body systems. *Phys. Rev. Lett.*, 121:060601, Aug 2018.
- [18] Jordan S Cotler, Guy Gur-Ari, Masanori Hanada, Joseph Polchinski, Phil Saad, Stephen H Shenker, Douglas Stanford, Alexandre Streicher, and Masaki Tezuka. Black holes and random matrices. *Journal of High Energy Physics*, 2017(5):118, 2017.
- [19] Xiao Chen and Andreas W. W. Ludwig. Universal spectral correlations in the chaotic wave function and the development of quantum chaos. *Phys. Rev. B*, 98:064309, Aug 2018.
- [20] C. W. von Keyserlingk, Tibor Rakovszky, Frank Pollmann, and S. L. Sondhi. Operator hydrodynamics, otocs, and entanglement growth in systems without conservation laws. *Phys. Rev. X*, 8:021013, Apr 2018.
- [21] Vedika Khemani, Ashvin Vishwanath, and David A. Huse. Operator spreading and the emergence of dissipative hydrodynamics under unitary evolution with conservation laws. *Phys. Rev. X*, 8:031057, Sep 2018.
- [22] Adam Nahum, Sagar Vijay, and Jeongwan Haah. Operator spreading in random unitary circuits. *Physical Review X*, 8(2):021014, 2018.
- [23] Tibor Rakovszky, Frank Pollmann, and C. W. von Keyserlingk. Diffusive hydrodynamics of out-of-time-ordered correlators with charge conservation. *Phys. Rev. X*, 8:031058, Sep 2018.
- [24] A. I. Larkin and Y. N. Ovchinnikov. Quasiclassical Method in the Theory of Superconductivity. *Soviet Journal of Experimental and Theoretical Physics*, 28:1200, June 1969.
- [25] Igor L. Aleiner, Lara Faoro, and Lev B. Ioffe. Microscopic model of quantum butterfly effect: Out-of-time-order correlators and traveling combustion waves. *Annals of Physics*, 375:378 – 406, 2016.
- [26] Brian Swingle, Gregory Bentsen, Monika Schleier-Smith, and Patrick Hayden. Measuring the scrambling of quantum information. *Phys. Rev. A*, 94:040302, Oct 2016.
- [27] Efim B. Rozenbaum, Sriram Ganeshan, and Victor Galitski. Lyapunov exponent and out-of-time-ordered correlator’s growth rate in a chaotic system. *Phys. Rev. Lett.*, 118:086801, Feb 2017.
- [28] Yingfei Gu and Alexei Kitaev. On the relation between the magnitude and exponent of otocs. *Journal of High Energy Physics*, 2019(2):75, 2019.
- [29] Juan Maldacena and Douglas Stanford. Remarks on the sachdev-ye-kitaev model. *Phys. Rev. D*, 94:106002, Nov 2016.
- [30] Debanjan Chowdhury and Brian Swingle. Onset of many-body chaos in the $o(n)$ model. *Phys. Rev. D*, 96:065005, Sep 2017.
- [31] Eugeniu Plamadeala and Eduardo Fradkin. Scrambling in the quantum lifshitz model. *Journal of Statistical Mechanics: Theory and Experiment*, 2018(6):063102, jun 2018.
- [32] Balázs Dóra and Roderich Moessner. Out-of-time-ordered density correlators in luttinger liquids. *Phys. Rev. Lett.*, 119:026802, Jul 2017.
- [33] Shenglong Xu and Brian Swingle. Locality, quantum fluctuations, and scrambling. *Phys. Rev. X*, 9:031048, Sep 2019.
- [34] Ivan Kukuljan, Sašo Grozdanov, and Tomaž Prosen. Weak quantum chaos. *Phys. Rev. B*, 96:060301, Aug 2017.
- [35] David J. Luitz and Yevgeny Bar Lev. Information propagation in isolated quantum systems. *Phys. Rev. B*, 96:020406, Jul 2017.
- [36] Douglas Stanford. Many-body chaos at weak coupling. *Journal of High Energy Physics*, 2016(10):9, 2016.
- [37] Aavishkar A. Patel, Debanjan Chowdhury, Subir Sachdev, and Brian Swingle. Quantum butterfly effect in weakly interacting diffusive metals. *Phys. Rev. X*, 7:031047, Sep 2017.
- [38] Yunxiang Liao and Victor Galitski. Nonlinear sigma model approach to many-body quantum chaos: Regularized and unregularized out-of-time-ordered correlators. *Phys. Rev. B*, 98:205124, Nov 2018.
- [39] Sašo Grozdanov, Koenraad Schalm, and Vincenzo Scopelitti. Kinetic theory for classical and quantum many-body chaos. *Phys. Rev. E*, 99:012206, Jan 2019.
- [40] Daniel A. Roberts and Brian Swingle. Lieb-robinson bound and the butterfly effect in quantum field theories. *Phys. Rev. Lett.*, 117:091602, Aug 2016.
- [41] Patrick Hayden and John Preskill. Black holes as mirrors: quantum information in random subsystems. *Journal of High Energy Physics*, 2007(09):120–120, sep 2007.
- [42] Winton Brown and Omar Fawzi. Decoupling with random quantum circuits. *Communications in Mathematical Physics*, 340(3):867–900, 2015.
- [43] A closely related quantity has been considered in the past in Ref. [34]. There, the focus was on the late-time behavior of the OTOC.
- [44] Daniel A Roberts, Douglas Stanford, and Alexandre Streicher. Operator growth in the syk model. *Journal of High Energy Physics*, 2018(6):122, 2018.
- [45] Andrew Lucas. Non-perturbative dynamics of the operator size distribution in the sachdev-ye-kitaev model. *Journal of Mathematical Physics*, 61(8):081901, 2020.
- [46] Daniel Gottesman. The heisenberg representation of quantum computers. *arXiv preprint quant-ph/9807006*, 1998.
- [47] See Supplementary Material.
- [48] U. Schollwöck. The density-matrix renormalization group in the age of matrix product states. *Annals of Physics*, 326:96–192, 2011.
- [49] ITensor Library, <http://itensor.org/>.
- [50] Ronald Aylmer Fisher. The wave of advance of advantageous genes. *Annals of eugenics*, 7(4):355–369, 1937.
- [51] AN Kolmogorov, IG Petrovsky, and NS Piskunov. Investigation of the equation of diffusion combined with increasing of the substance and its application to a biology problem. *Bull. Moscow State Univ. Ser. A: Math. Mech*, 1(6):1–25, 1937.

Supplementary Material

S1. GENERALIZED CLIFFORD CIRCUIT

In Fig. S1 we present additional results for the generalized Clifford circuit, in which CNOT gates are replaced by two-qubit operators defined in Eq. (7) in the main text. Here, an average over 400 circuit realizations was performed, and an averaged OTOC over the different pauli operators, i.e. $\propto \sum_{\mu, \nu=x,y,z} [\sigma_i^\mu(t), \sigma_j^\nu]^2$ was calculated. It can be seen that the behavior of the iOTOC in this case is similar to the one observed for the special Clifford circuit in Fig. 3 in the main text. In particular, a prolonged regime of exponential growth can be clearly seen for small values of r , and the scaling of the crossover time, expected from Eq. (3) in the main text, holds.

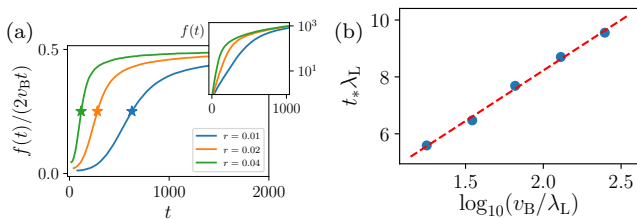


FIG. S1. (a) The OTOC density, i.e. $f(t)/(2v_B t)$, for different values of r in the generalized Clifford circuit with $p = 1$. Crossover time at which the OTOC density reaches half of its saturation value is marked by a star. The inset shows the iOTOC on a log scale. (b) Scaling of the crossover time expected from Eq. (3) in the main text.

S2. SPATIAL STRUCTURE OF THE OTOC AND HYDRODYNAMIC EQUATIONS FOR $C(x, t)$

In the main text we focused on the integrated OTOC, arguing that this quantity allows for an easier identification and characterization of the scrambling time in systems with local structure. For completeness, here we discuss the spatial structure of the OTOC in the circuit under investigation.

S2.1. Local OTOCs

In Fig. S2, we show the local OTOC $C_{i,j}(t) = \langle [\sigma_i^z(t), \sigma_j^x]^2 \rangle$ as function of time, at different positions along the 1D chain, obtained for the special Clifford circuit with $p = 1$ and $r = 0.05$. For $j = i$, an exponential growth of the OTOC at early times can be clearly seen. For $j \neq i$ the OTOC vanishes identically before the arrival of the light cone at time $t = v_B |j - i|$. While for $|j - i| \ll t_*/v_B$ we expect a regime of exponential growth to be present, for $|j - i| \gtrsim t_*/v_B$ this is no longer the case as can be seen in the Figure.

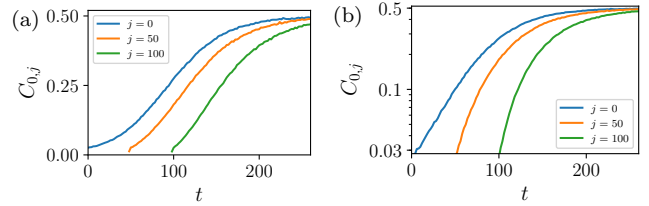


FIG. S2. Local OTOC $C_{0,j}$ probed at different values of j on a linear scale in (a) and a log scale in (b), obtained for the special Clifford circuit with $p = 1$ and $r = 0.05$.

S2.2. Scaling of v_B with λ_L in the diffusive circuit

In the main text, we argued, that to allow for a parametrically large regime of exponential growth of the OTOC, a diverging ratio of v_B/λ_L is required. When the dynamics in the absence of interactions is diffusive (which in the case of the random circuit model under study occurs when $p < 1$), a finite scattering rate (i.e. a finite λ_L) is required to generate a well-defined butterfly velocity, v_B . It is thus important to verify the scaling of v_B with λ_L still allows for a diverging ratio v_B/λ_L in the $\lambda_L \rightarrow 0$ limit. In Fig. S3 we show that in the small λ_L regime, the scaling is $v_B \propto \sqrt{\lambda_L}$ as expected [37].

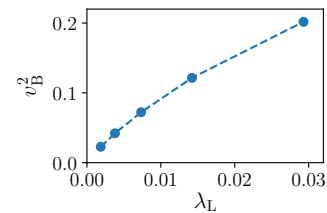


FIG. S3. Scaling of the butterfly velocity v_B with the scattering rate λ_L for a diffusive Clifford circuit with $p = 0.9$.

S2.3. Hydrodynamic equations for $C(x, t)$

S2.3.1. Regime of validity of the hydrodynamic equations

In deriving the hydrodynamic equations we make the same assumption as in the master equation, that the creation and annihilation events of σ^z operators in the operator string, due to CNOT gates, are dilute and uncorrelated. In a correlated collision two σ^z operators that were generated by a CNOT gate collide again, resulting in the annihilation of one of them. In other words, a correlated collision yields a closed loop of world lines of two initially generated σ^z operators. The hydrodynamic equation is valid when the probability of correlated collisions is negligible, i.e. much smaller than the probability

of the uncorrelated collisions where the world lines do not form closed loops. Below we estimate the probability of correlated collision in the ballistic and diffusive circuits separately.

Ballistic case ($p = 1$): After two σ^z operators are created by a CNOT gate, they start propagating in opposite directions under the action of SWAP gates. The probability that this CNOT gate generated a correlated collision is then equal to the probability that the two operators undergo a single collision each before meeting again, which is of order unity, times the probability that the two operators collide upon meeting, which is r . Therefore, in the limit $r \rightarrow 0$ the probability to generate a correlated collision event vanishes, and the hydrodynamic description is justified.

Diffusive case ($p < 1$): In this case, in addition to CNOT gates, backscattering events can be generated by missing SWAP gates. We consider the limit $1 \ll 1/(1-p) \ll 1/r$, so that diffusive backscatterings dominate. We ask once again what is the probability for two σ^z operators to meet and collide with each other before colliding independently. Recall that the typical time between consecutive backscatterings due to missing SWAP gates is $\tau_p \sim (1-p)^{-1}$. Therefore, the probability for the two σ^z operators to meet again without undergoing a collision is given by $p_{\text{meet}} \sim (1-r)^{2\tau_p}$. In the regime $\tau_p \ll \tau_r$ multiple meetings of the operators can occur before a CNOT gate acts on them. Summing over all such trajectories we obtain that the probability to generate a correlated collision is $p_{\text{meet}} [\sum_{n=0}^{\infty} (1-r)^n p_{\text{meet}}^n] r \sim (1-p)$. In other words, in the regime $1-p \gg r$, the validity of the hydrodynamic equation is limited by smallness of $1-p$.

S2.3.2. Hydrodynamic equations for the ballistic circuit

In the ballistic circuit, the OTOC density $C(x, t)$ decouples into left and right moving densities, $C_L(x, t)$ and $C_R(x, t)$, respectively. Hydrodynamic equations for the evolution of these densities are given by,

$$\begin{aligned} \frac{\partial C_R}{\partial t} &= -v_{B,0} \frac{\partial C_R}{\partial x} + r [C_L(1 - C_R) - C_L C_R] \\ \frac{\partial C_L}{\partial t} &= v_{B,0} \frac{\partial C_L}{\partial x} + r [C_R(1 - C_L) - C_L C_R]. \end{aligned} \quad (\text{S1})$$

Note that operators on neighboring sites have opposite propagation directions. Hence, a right moving operator can be generated only from a left moving one, and annihilation occurs only when left and right moving operators meet - in this case one of them (the one corresponding to the control qubit) is annihilated.

We now argue that these coupled equations admit a traveling wave solution, with no front broadening. We start by considering a solution of the form $C_{L,R} = C_{L,R}(x - v_B t)$, which turns the set of equations in (S1) into coupled non-linear ordinary differential equations. There are two fixed point solutions for these equations,

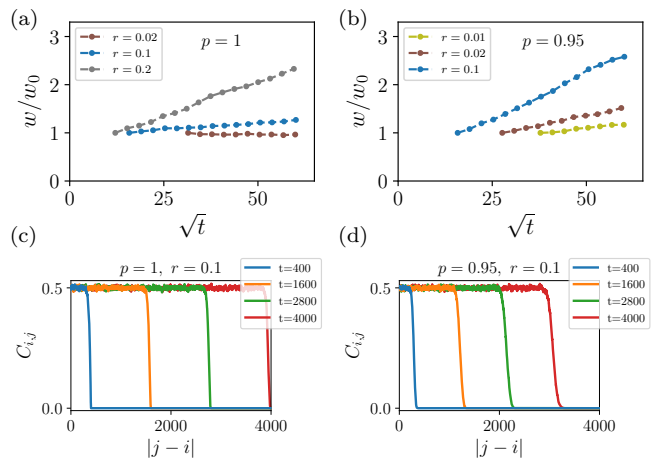


FIG. S4. Front broadening in the special Clifford random circuit model. (a,c) The width of the front as function of time, normalized by the width of the front at the time when the OTOC in the bulk reaches saturation, w_0 , for $p = 1$ in (a) and $p = 0.95$ in (b). The local OTOC at different times for $p = 1, r = 0.1$ in (c) and for $p = 0.95, r = 0.1$ in (d).

$C_{L,R} = 0$ and $C_{L,R} = 1/2$. Performing a linear stability analysis around these fixed points, we find that while the former point is a saddle point and thus unstable, the latter one is a stable solution, as long as $v_B > v_{B,0}$. While this suggests that multiple velocities are possible for the propagation of the wave, as discussed in Refs. [25, 33], the physical velocity corresponds to the lower bound on the allowed velocities. Note however that the limit $v_B \rightarrow v_{B,0}$ is singular, signaling a breakdown of the continuum limit. Hence, we expect the velocity of propagation to be $v_B = v_{B,0} + v_\epsilon$, with the cutoff for v_ϵ being set by lattice-scale microscopic parameters.

S2.3.3. Hydrodynamic equation for the diffusive circuit

In the diffusive case the total OTOC density $C(x, t)$ satisfies

$$\frac{\partial C}{\partial t} = D \frac{\partial^2 C}{\partial x^2} + r [C(1 - C) - C^2], \quad (\text{S2})$$

where D is the diffusion constant. This differential equation is known as the FKPP equation [50, 51] which, similarly to the equations for the ballistic case, admits a traveling wave solution. Following a similar analysis to the one outlined in Ref. [25], we find that the physical velocity for the propagation of the wave in this case is given by $v_B = 2\sqrt{Dr}$, in qualitative agreement with the behavior seen in Fig. S3.

S2.3.4. Numerical analysis of front broadening

We now present numerical results for the broadening of the front in our random circuit model. A well-defined

front develops once the OTOC reaches saturation value in the bulk, which in the main text was denoted by C_{sat} . We define the front as the region in space where the OTOC varies between $0.2C_{\text{sat}}$ and $0.8C_{\text{sat}}$. At the time the OTOC in the bulk reaches saturation value, the front has a finite width that we denote by w_0 (this width is increasing with v_B/r). In Figs. S4(a,b) we plot the width w normalized by w_0 as function of time, for $p = 1$ and $p = 0.95$ for different values of r . As can be seen, the front does not broaden (or broadens very slowly) in the

limit of $p \rightarrow 1, r \rightarrow 0$. This is indeed the regime in which we expect the hydrodynamic equations to hold, and for a traveling wave solution without front broadening to exist. In Figs. S4(c,d) the front itself is shown at different times for $r = 0.1$, and $p = 1, 0.95$. Here, to reduce the noise, a convolution with a uniform kernel of size 10 sites was performed (note that since the size of the kernel is small compared to the width of the front this does not alter the results). It can be explicitly seen that while there is no broadening for the ballistic case with $p = 1$, the front does broaden for $p = 0.95$ for this value of r .